ADVANCED FUNCTIONAL MATERIALS
www.afm-journal.de

Realization of Fully High-Spin State and Strong Ferromagnetism in $LaCoO_3$ Monolayer

Junhua Liu, Liang Si, Qinghua Zhang, Xiao Wang, Jessica Freese, Grant Harris, Mei Wu, Xinxin Zhang, Ting Lin, Ronny Sutarto, Javier Herrero-Martín, Charles Guillemard, Manuel Valvidares, Lin Li, Xiaofei Gao, Yaoyao Ji, Zhixiong Deng, Yuhao Hong, Long Wei, Yulin Gan, Lingfei Wang, Guanglei Cheng, Peng Gao, Lin Gu, Jiandi Zhang, Zhiwei Hu, Liu Hao Tjeng, Robert J. Green, Kai Chen,* and Zhaoliang Liao**

Perovskite $LaCoO_3$ is a subject of extensive and ongoing investigation due to the delicate competition between high-spin (HS) and low-spin (LS) states of Co^{3+}. On the other hand, their indistinct free energy boundary poses a significant challenge to annihilate the magnetically/electrically inert LS Co^{3+} for yielding fully HS state. Here, electronic transformation from the conventional isovalent mixed HS/LS state ($La[Co^{3+}_{HS}, Co^{3+}_{LS}]O_3$) into an unprecedented aliovalent fully HS state ($La[Co^{3+}_{HS}, Co^{2+}_{HS}]O_3$) is demonstrated in monolayer $LaCoO_3$ confined by 5d $SrIrO_3$ slabs via atomically constructing $SrIrO_3/LaCoO_3$ superlattices. Excitingly, this emergent fully HS $La[Co^{3+}_{HS}, Co^{2+}_{HS}]O_3$ monolayer exhibits not only remarkable 2D ferromagnetism beyond the Mermin–Wagner restriction, but also larger magnetization ($\approx 1.8\mu_B$/Co) and higher Curie temperature (above 100 K) than that of conventional $La[Co^{3+}_{HS}, Co^{3+}_{LS}]O_3$ thick film and any previously reported oxide-based monolayer ferromagnets. Furthermore, Ir/Co hybridization driven orbital reconstruction with polarization beyond standard crystal field expectations is observed, which is supported by DFT calculations. The findings not only expand the electronic phase domains of LCO into fully HS state, but also provide a fresh platform for investigating the 2D magnetic physics under strongly spin-orbit coupled regime and developing new 2D spintronic devices.

1. Introduction

Spin-state crossover, where the spin state of an ion can be switched by specific stimuli such as temperature,[1] strain,[2] and light excitation,[3] has continuously attracted significant scientific and technological interest owing to remarkable spin-state-controlled properties. Such a phenomenon involves a wide range of fields including magnetics,[2,4] optoelectrics,[3a] molecular electronics,[5] metalorganic chemistry[6] and even geoscience,[7] manifesting diverse functionalities[3a,8] such as non-volatile memory, switching, displaying, and energy transduction. 3d cobaltate is an intriguing and representative system with spin-state crossover, where the prototyped perovskite counterpart, $LaCoO_3$ (LCO), has been a subject of increasing attention for over 50 years owing to the high correlation between its magnetism and spin state.[1,2,4,9] The spin state of Co^{3+} mainly depends on the competition between the splitting of the crystal field (Δ_{CF}) and Hund's exchange (J_H).[1,2b,9d,e,10] External stimuli can tip the

J. Liu, L. Li, X. Gao, Y. Ji, Z. Deng, Y. Hong, L. Wei, Y. Gan, K. Chen, Z. Liao
National Synchrotron Radiation Laboratory
University of Science and Technology of China
Hefei 230026, China
E-mail: kaichen2021@ustc.edu.cn; zliao@ustc.edu.cn

L. Si
School of Physics
Northwest University
Xi'an 710127, China

L. Si
Institute of Solid State Physics
TU Wien
Vienna 1040, Austria

Q. Zhang, T. Lin, J. Zhang
Beijing National Laboratory for Condensed Matter Physics
Institute of Physics
Chinese Academy of Sciences
Beijing 100190, China

X. Wang, Z. Hu, L. H. Tjeng
Max Planck Institute for Chemical Physics of Solids
Nöthnitzer Straβe 40, 01187 Dresden, Germany

J. Freese, G. Harris, R. J. Green
Department of Physics and Astronomy and Stewart Blusson Quantum Matter Institute
University of British Columbia
Vancouver, BC V6T1Z4, Canada
E-mail: robert.green@usask.ca

The ORCID identification number(s) for the author(s) of this article can be found under https://doi.org/10.1002/adfm.202401859

DOI: 10.1002/adfm.202401859

competing balance, leading to a spin-state crossover from the low-spin (LS) Co^{3+} ($t_{2g}^6 e_g^0$, $S = 0$) to the mixed state with high-spin (HS) Co^{3+} ($t_{2g}^4 e_g^2$, $S = 2$).[1a,2b,9b,11] The LS Co^{3+} possessing no electronic/magnetic activity is undesirable,[1a,12] but there is a significant challenge to completely annihilate it thereby leaving only the HS state due to their symbiotic nature caused by the close and ambiguous free energy boundary between HS Co^{3+} and LS Co^{3+} in LCO.[1a] Therefore, as observed in previously reported LCO, regardless of being modified by strain, temperature, or doping/substitution, all Co^{3+} exhibited a mixed HS/LS state.[1,2,4a,9b,11a,13] To expand the electronic phase domains and gain insight into the manifestation of LCO with fully HS state, other knobs to effectively suppress the LS Co^{3+} are highly desired.

The main fundamental challenge for the realization of fully HS state lies in the six-coordinated Co^{3+} in LCO where Δ_{CF} is extremely close to J_H. In comparison, fully HS Co^{3+} has been observed in lower-coordinated cobaltates, such as the $Sr_2CoO_3Cl_2$ with[CoO_5] pyramids[10] and $YBaCo_4O_7$ with [CoO_4] tetrahedra,[14] owing to weaker Δ_{CF} arising from reduced oxygen coordination. Therefore, the question will be, in stoichiometric $LaCoO_3$ with the [CoO_6] octahedral framework, how to fully suppress LS Co^{3+}. Most previous studies about LCO mainly focus on bulk or relatively thick films. Given the highly focused 2D materials, where electron correlation and symmetry breaking are fundamentally different due to the low-dimensional effects and interface interactions, it would be interesting to gain insight into the effect of reduced dimensionality and heterointerface effects on spin-state crossover. Constructing heterostructure allows interweaving various complex interplays from different oxides as well as inversion symmetry breaking,[15] providing unprecedented opportunities for tailoring the electronic states of individual components.[16] Advanced epitaxial techniques can artificially and precisely customize the dimensions and interface environment of LCO by introducing specific functional layers, thereby potentially breaking bottleneck of current research on LCO spin-state crossover.

Here, we rationally grew high-quality LCO monolayers by synthesizing superlattices composed of $SrIrO_3$ (SIO) and LCO to introduce charge transfer, spin-orbit coupling (SOC) and orbital hybridization through the interface as well as the enhanced electron correlations at 2D limit. We are able to fully suppress the LS Co^{3+} and therefore to realize an unprecedented fully HS state ($La[Co^{3+}_{HS}, Co^{2+}_{HS}]O_3$) in the monolayer limit of LCO in such a superlattice. This emergent species $La[Co^{3+}_{HS}, Co^{2+}_{HS}]O_3$, significantly different from the $SrTiO_3$-confined LCO monolayer that possesses a mixed HS/LS state and nonmagnetic ground state, displays not only strong 2D ferromagnetism but also orbital reconstruction with large and anomalous polarization indicated by our synchrotron spectroscopy together with theoretical calculations. These results suggest a nontrivial 2D HS system with possible multiple coexisting quantum orders, which provides a novel platform for exploring complex interplay and magnetic physics at the 2D limit under strong SOC regime and new applications in 2D electronic devices. Furthermore, our study will provide deep insight into the understanding of spin state transitions and pave a path for engineering the 2D epitaxial magnet for practical application.

2. Results

2.1. Emergent Fully High-Spin State in $LaCoO_3$ Monolayer

A series of high-quality $[SIO_5/LCO_n]_{10}$ (S_5L_n, n = 1–10 uc) and $[SIO_1/LCO_1]_{20}$ (S_1L_1) SLs were grown on TiO_2-terminated $SrTiO_3$ (STO) (001) substrates. Expected periodic stacking was revealed by high-angle annular dark-field scanning transmission electron microscopy (HAADF-STEM) measurements (see **Figure 1a**). The clear contrast between La (Sr) and Ir (Co) is evidenced, demonstrating abrupt interfaces and coherent growth, which is consistent with results from X-ray diffraction (XRD) and reciprocal space mapping (RSM) (see Figure S1, Supporting Information). These measurements consistently confirm that a high-quality SIO-confined LCO monolayer was prepared. X-ray absorption spectra (XAS) measurements were conducted to detect the electronic structure of LCO with varied thickness. The appearance of Co^{2+} and the elevation of Ir valence together unravel the charge transfer process,[17] i.e., $Ir^{4+} + Co^{3+} \rightarrow Ir^{5+} + Co^{2+}$ (see Figure S2, Supporting Information). This is in good agreement with the theoretically proposed charge transfer model at perovskite oxide interfaces.[18] Such a charge transfer at the interface cooperating with other complex interplays modifies the electronic structure

J. Freese, G. Harris, R. J. Green
Department of Physics & Engineering Physics
University of Saskatchewan
Saskatoon S7W0R4, Canada

M. Wu, X. Zhang, P. Gao
Electron Microscopy Laboratory
School of Physics and International Center for Quantum Materials
Peking University
Beijing 100871, China

T. Lin
School of Physical Sciences
University of Chinese Academy of Sciences
Beijing 100049, China

R. Sutarto
Canadian Light Source
Saskatoon, SK S7N2V3, Canada

J. Herrero-Martín, C. Guillemard, M. Valvidares
ALBA Synchrotron Light Source
Cerdanyola del Vallès, Barcelona 08290, Spain

L. Wang
Hefei National Research Center for Physical Sciences at Microscale
University of Science and Technology of China
Hefei 230026, China

G. Cheng
CAS Key Laboratory of Microscale Magnetic Resonance and School of Physical Sciences
University of Science and Technology of China
Hefei 230026, China

G. Cheng
Hefei National Laboratory
Hefei 230088, China

L. Gu
Beijing National Center for Electron Microscopy and Laboratory of Advanced Materials
Department of Materials Science and Engineering
Tsinghua University
Beijing 100084, China

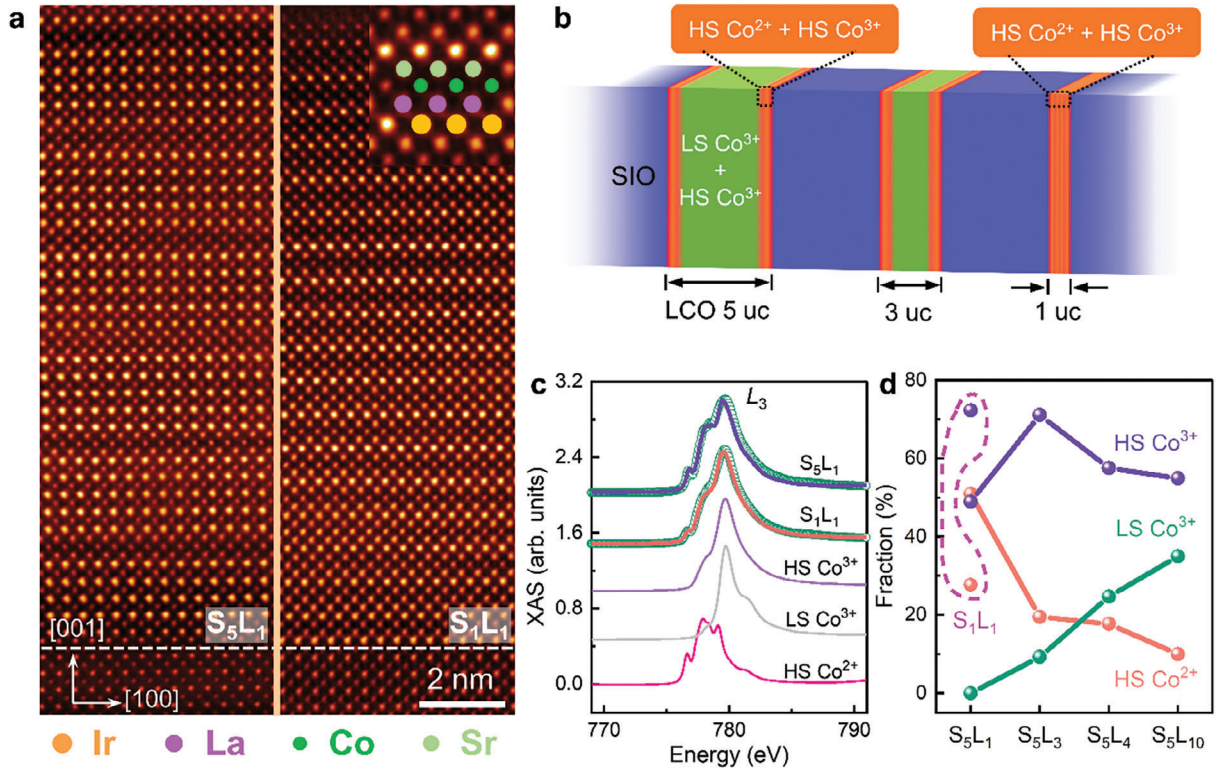

Figure 1. Evolution of nominal Co spin/electronic states. a) HAADF-STEM results of S_5L_1 and S_1L_1. The inset is a zoom view of S_1L_1 image. b) Schematic of spin state profile of Co ions. There are almost only HS Co^{2+}/Co^{3+} at interface, different from the bulk regime (green, dominated by HS/LS Co^{3+}). c) Co-L_3 XAS fitting results of LCO monolayer SLs, where the feature of LS Co^{3+} (right shoulder) is absent. The spectra line-shape of S_5L_1 and S_1L_1 can be simulated by a linearly combination of only HS Co^{3+} and HS Co^{2+}, where 49% HS Co^{3+} and 51% HS Co^{2+} are for S_5L_1, and 72.3% HS Co^{3+} and 27.7% HS Co^{2+} are for S_1L_1. Reference HS Co^{3+}, LS Co^{3+}, and HS Co^{2+} XAS spectra are the experiment results of $Sr_2Co_{0.5}Ir_{0.5}O_4$, $NdCaCoO_4$ and CoO, respectively.[19] d) Fractions of HS Co^{3+}, LS Co^{3+} and HS Co^{2+} in superlattices for varied LCO thickness.

of interfacial area of LCO slabs, eventually giving rise to a fully HS state in the monolayer limit, where the spin state profile can be schematically illustrated as shown in Figure 1b. In detail, the contributions of each XAS component were deconvoluted by a linear combination analysis,[12b] including HS Co^{2+}, HS Co^{3+} and LS Co^{3+} reference spectra (extracted from ref. [19]) as exemplified in Figure 1c and Figure S3 (Supporting Information). The fitting results are summarized in Figure 1d and Table S1 (Supporting Information), where the percentage of HS Co^{2+} increases following an inverse proportional dependence on thickness n, consistent with the interface charge transfer scenario (see discussion in Note S4, Supporting Information). In contrast, the percentage of LS Co^{3+} shows a monotonic decrease, and thus a significant number of HS Co ions are nominally accumulated with reducing LCO thickness. Ultimately, all the Co ions exhibit the HS state, causing the LCO monolayer (S_5L_1 and S_1L_1) to transform into an emergent monolayer species $La[Co^{3+}_{HS}, Co^{2+}_{HS}]O_3$, where their XAS spectra can be well simulated by a linear combination of only HS Co^{2+} and HS Co^{3+} reference spectra (see Figure 1c).

2.2. Emergent Strong Ferromagnetism in $LaCoO_3$ Monolayer

Magnetic characterizations were performed for S_5L_n to elucidate the magnetism of LCO. Normally, the magnetization decays with reducing film thickness due to the "dead layer" effect[13,20] and Mermin–Wagner restriction[21] then a ferromagnetic–paramagnetic transition occurs when approaching monolayer thickness as shown by the reference $[STO_5/LCO_1]_{10}$ (T_5L_1) in **Figure 2a**. With respect to S_5L_n SLs, on the contrary, the ferromagnetism not only surprisingly survives when down to monolayer (S_5L_1), but is also obviously enhanced compared to thick LCO films. Previous reports have demonstrated that ferromagnetic LCO can induced unsaturated anomalous Hall effect (AHE) in the originally paramagnetic SIO possessing strong SOC by magneto-proximity effect.[17a,22] Therefore, the observed unsaturated AHE in S_5L_1 up to 100 K (see Figure 2b) conversely indicates a robust ferromagnetism in the LCO monolayer.

The intrinsic ferromagnetism of ultrathin LCO (n = 1–3) was further probed by Co-$L_{2,3}$ X-ray magnetic circular dichroism spectra (XMCD). As shown in Figure 2c, the upper panel displays XAS recorded with circularly polarized X-rays with the polarization parallel (μ^+) and antiparallel (μ^-) to the magnetic field direction. The spectral difference ($\mu^+ - \mu^-$, namely XMCD) shows finite signals (for raw spectra see Figure S5, Supporting Information), confirming the ferromagnetism of ultrathin LCO. Their ferromagnetism is collectively contributed by both HS Co^{2+} and HS Co^{3+}, as shown by comparing the XMCD line-profile with reference spectra.[17c] For instance, the experimental XMCD line-profile in

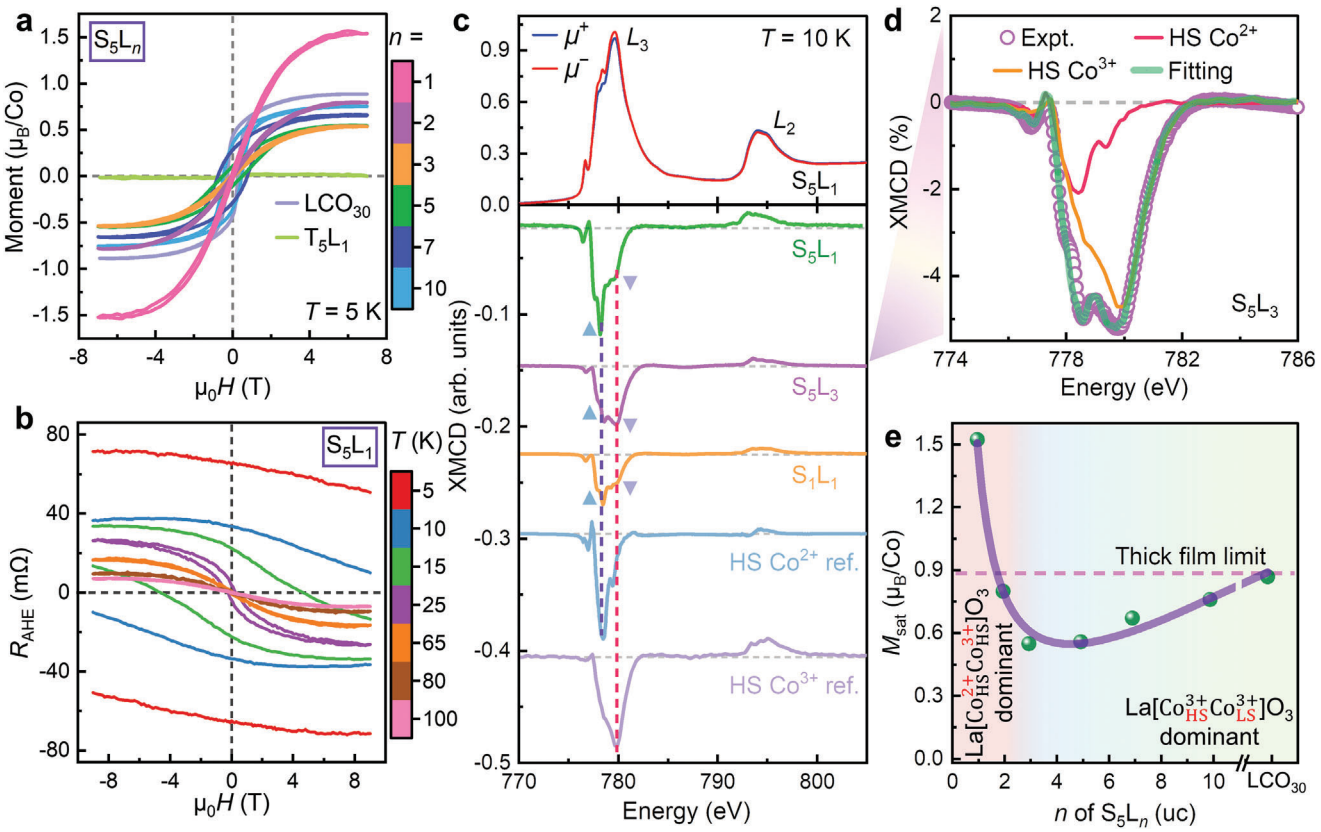

Figure 2. Survival and enhanced ferromagnetism as LCO down to monolayer. a) In-plane *M-H* curves of S_5L_n, T_5L_1 and 30-uc $LaCoO_3$ film (LCO_{30}). b) AHE resistance (R_{AHE}) hysteresis of S_5L_1. See Experimental Section for measurement details. c) Co-$L_{2,3}$ XMCD results at 10 K with applied field (6T) perpendicular to sample plane, where the reference spectra of HS Co^{3+} and HS Co^{2+} are the experimental XMCD results of Sr_2CoIrO_6[17c] and CoO, respectively. The signal magnitudes of XMCD, defined as a percentage of the maximum of corresponding Co-L_3 edge, were 8.9% for S_5L_1, 4.9% for S_5L_3 and 4.5% for S_1L_1. By linearly combining the reference spectra of HS Co^{3+} and HS Co^{2+}, the XMCD of S_5L_3 is almost perfectly reproduced in d,e) Evolution of Co saturated moment (M_{sat}) with LCO thickness at 5 K.

S_5L_3 can be well reproduced by a linear combination of reference spectra, as shown in Figure 2d. The non-monotonic evolution of saturated moment (M_{sat}) with LCO thickness (extracted from Figure 2a) is plotted in Figure 2e, where a dead-layer-like phenomenon is observed for n = 3–10, that is, magnetism weakens with reducing thickness. However, the surviving and counterintuitively enhanced magnetization can be observed when thinning LCO to 2D limit (n ≤2), which is even much larger than that of thick LCO films,[23] verified as well by XMCD in Figure 2c.

Element-specific resonant soft X-ray reflectometry (RSXR),[24] an advanced technique to obtain the magnetic as well as the chemical/structural depth profile of the sample with very high precision, was used to investigate global magnetization distribution of S_5L_1 as illustrated in **Figure** 3a. A strong asymmetry in dichroic circular polarized X-ray spectra was fitted (see Figure S6, Supporting Information) to yield the periodic magnetization (M) profile spatially corresponding to the LCO slabs (see Figure 3b), confirming the long-range ferromagnetic order in the LCO monolayer. Notably, the finite magnetic signal under 100 K demonstrates a Curie temperature beyond corresponding thick film (≈85 K), which is consistent with the AHE measurement in Figure 2b, confirming the high-ordering temperature of $La[Co^{3+}_{HS}, Co^{2+}_{HS}]O_3$.

The enhanced Co moment in S_5L_1 can therefore be explained by the crossover from conventional mixed HS/LS states to fully HS state as the thickness of LCO decreases (see Figure 1d). The LS Co^{3+} exhibits a non-magnetic electron configuration (S = 0), while the HS Co^{3+} (S = 2) possesses a magnetic moment of 4μ_B/Co. For conventional thick LCO ($La[Co^{3+}_{HS}, Co^{3+}_{LS}]O_3$), the mixing of LS Co^{3+} and HS Co^{3+} yields a small nominal moment of ≈1μ_B/Co. However, for the SIO-confined LCO monolayer, the non-magnetic LS Co^{3+} is depleted completely during the charge transfer process, emerging the fully HS monolayer species $La[Co^{3+}_{HS}, Co^{2+}_{HS}]O_3$ as a combination of HS Co^{3+} and HS Co^{2+} ($t_{2g}^5e_g^2$, S = 3/2, m = 3μ_B/Co), as shown in Figure 1b. Consequently, it exhibits an enhanced nominal moment (≈1.8μ_B/Co), which is approximately twice as large as that of the single LCO_{30} thick film.

2.3. Orbital Occupancy Anomaly and Strong Polarization

X-ray linear dichroism (XLD, defined as $I_{E//ab}-I_{E//c}$) spectra of the Co-$L_{2,3}$ edge are used to uncover the valence orbital states. As shown in **Figure** 4a (left panel), T_5L_1 with electronic structure of $La[Co^{3+}_{HS}, Co^{3+}_{LS}]O_3$ exhibits an almost zero XLD signal,

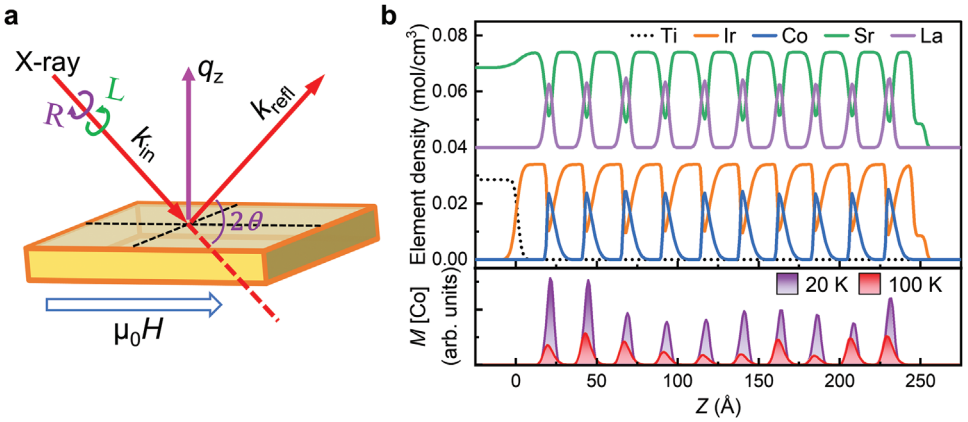

Figure 3. Ferromagnetism beyond 100 K in LCO monolayer. a) Experimental set-up sketch of RSXR measurements, where a 0.6 T magnetic field was applied in-plane during the measurement. b) Magnetic and element profiles in S_5L_1 at 20 and 100 K along the [001] direction (Z), where the terminated LCO was capped by additional 3 uc SIO for avoiding degradation. For clarity, the element density of A-site ions, including La and Sr, is offset vertically by 0.04.

indicating degenerate Co e_g and t_{2g} orbitals instead of the usual tensile strain-driven energy level splitting (XLD <0). However, for S_5L_1, a significant positive XLD (≈10%) was observed (see Figure 4a, right panel), indicating a large orbital polarization in the $La[Co^{3+}_{HS}, Co^{2+}_{HS}]O_3$. The positive XLD signal demonstrates that the in-plane (IP) orbital energy level is higher than that of the out-of-plane (OOP) orbital, even under tensile strain. We further conducted simulations on the anomaly of the orbital level through multiplet calculations (see Note S7, Supporting Information), which show good agreement with the experimental results, confirming the unforeseen orbital level inversion in the SIO-confined LCO monolayer. Here, might as well define that T_5L_1 with degenerate Co e_g and t_{2g} orbitals holds an effective tetragonal ratio $(c/a)_{eff}$ ≈1, the preferred OOP population in S_5L_1 then suggests that it has $(c/a)_{eff} > 1$ and thus the c-axis of LCO monolayer in S_5L_1 could be longer than that in T_5L_1.

To investigate the effective tetragonal ratio further, the lattice profile is probed microscopically by HAADF-STEM. As shown by the profile of the OOP A–A distance (see Figure 4b; Figure S10, Supporting Information), the statistical c-axis length (d_c)

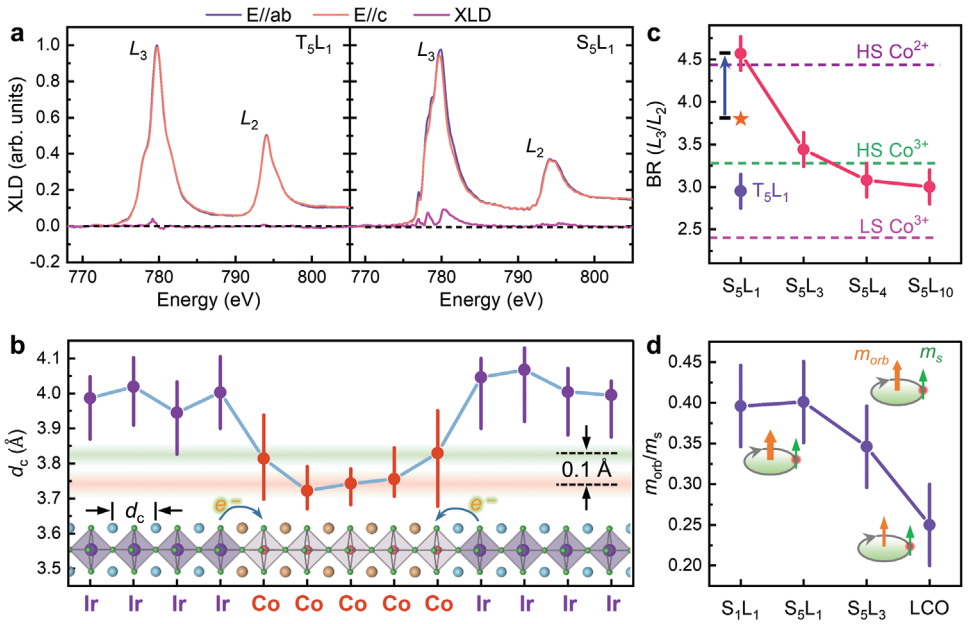

Figure 4. Anomalous orbital reconstruction and enhanced SOC. a) XLD results at Co-$L_{2,3}$ edge, which is defined as $I_{E//ab} - I_{E//c}$. b) Increased c-axis length (d_c) near interface in S_5L_5, which is characterized by the distance between two adjacent A-sites as illustrated by the inset. These results were obtained statistically from a 22 uc × 22 uc cross-section region of the HAADF image. c) Branching ratio (BR = L_3/L_2) extracted from Co-$L_{2,3}$ XAS, where the reference levels (dashed line) are derived from experimental spectra.[19] The orange five-pointed star denotes the calculated weighted average BR* based on the reference levels. d) Evolution of m_{orb}/m_s, where the data of LCO is extracted and processed from ref. [1a] The error bars of BR and m_{orb}/m_s are from the final state effects of the core level SOC and core-valence exchange interactions (multiplet effects) of Co ions.

of the interfacial LCO layer (3.83 Å) is ≈3% larger than that of the inner LCO layers (3.73 Å). Interface charge transfer from Ir to Co sites, as discussed above, is a possible cause for *c*-axis lattice expansion, which has been widely observed in interface charge transfer systems.[17b,25] Furthermore, our DFT calculations (as discussed below) show that strong orbital hybridization between Ir and Co ions reverses Co 3d levels, consistent with the XLD result. That is, interface charge transfer and Ir–Co orbital hybridization could synergistically cause the anomalies of the orbital levels and lattice expansion, leading to a reconstructed orbital state beyond the crystal field expectations.

2.4. Enhanced Spin-Orbit Coupling

Enhanced SOC, affording large magnetocrystalline anisotropy to resist fluctuation for reviving long-range ferromagnetic order, is verified by calculating the Co-$L_{2,3}$ XAS branching ratio[26] (BR = L_3/L_2, for details see Note S8, Supporting Information). As shown in Figure 4c, the BR monotonically increases with reducing LCO thickness, demonstrating the stronger BR in the interfacial LCO layer than in the bulk region. This can be interpreted as an increase in the fractions of HS Co^{2+} and HS Co^{3+} with large BR intuitively, consistent with the spin state profile shown in Figure 1b. Notably, BR is also associated with SOC $\langle\Sigma(l{\cdot}s)\rangle$ in addition to percentages of HS Co^{2+} and HS Co^{3+} (Co3d holes n_h) according to the formula[26] (BR−2)/(BR+1) = $\langle\Sigma(l{\cdot}s)\rangle/n_h$. The significantly enhanced BR cannot be simply described by the increasing fractions of HS Co^{2+} and HS Co^{3+} with strong SOC. The weighted average value (BR^*) of S_5L_1 derived from trivial HS Co^{2+} and HS Co^{3+} reference spectra[19] is shown by the orange five-pointed star in Figure 4c, which is much smaller than the experimental BR (red point). The large gap (indicated by the blue arrow) between them strongly suggests that the SOC $\langle\Sigma(l{\cdot}s)\rangle$ in the LCO monolayer is additionally enhanced when interfacing with SIO. In contrast, the STO-confined non-magnetic monolayer (T_5L_1) shows a BR value (or SOC) much smaller than that of ferromagnetic S_5L_1, indicating that enhanced SOC favors the ferromagnetic order in LCO monolayer.

The orbital-to-spin moment ratio (m_{orb}/m_s) can be calculated from the XMCD sum rules.[27] The m_{orb}/m_s systematically increased with thinning LCO (see Figure 4d; Table S2, Supporting Information), and its maximum (≈0.4) is observed in both S_1L_1 and S_5L_1. Given the total saturated moment of 1.8μ_B/Co in S_5L_1 (at 2 K), the unquenched orbital moment can be estimated to be m_{orb} = 0.51μ_B/Co. Furthermore, the XMCD results show that S_1L_1 possesses more HS Co^{3+} (less HS Co^{2+}) participation in the magnetic contribution than S_5L_1 yet has a similar m_{orb}/m_s as S_5L_1, indicating that the HS Co^{3+} possesses a comparable m_{orb}/m_s as HS Co^{2+}, or m_{orb}/m_s of both HS Co^{2+} and HS Co^{3+} is enhanced in the ferromagnetic LCO monolayer, consistent with the additionally enhanced SOC as discussed above.

2.5. DFT+U Calculations

DFT+U calculations were employed to investigate the electronic and magnetic properties of the LCO monolayers. Our calculations show that the ground state of the STO-strained LCO single film is ferromagnetic, while the ferromagnetic order collapses when LCO is confined by STO to monolayer thickness (T_5L_1, see Figure S13, Supporting Information). This finding is foreseeable and consistent with previous reports.[13] For the SIO-confined LCO monolayer (S_5L_1), strong interface electron transfer is observed from Ir to Co sites, consistent with our experimental results and previous reports.[17a,b,18] We further attempt to understand the coexistence of HS Co^{3+} and HS Co^{2+}, where three possible states can be derived as shown in Figure S14 (Supporting Information). **Figure 5**a,b shows the total and partial DOS of Co ions in S_5L_1 in the ground state (right panel in Figure 5c). Apparently asymmetric spin subbands are observed for both HS Co^{3+} and HS Co^{2+}, demonstrating ferromagnetism in the LCO monolayer.

We further observed strong hybridization between the localized Co3d orbital and itinerant Ir5d orbital. Generally, SIO (LCO) grown on STO suffers from compressive (tensile) strain, which causes the t_{2g} electrons in SIO (LCO) to tend to occupy out-of-plane d_{xz}/d_{yz} (in-plane d_{xy}) orbitals. The strong orbital hybridization and charge transfer between Ir and Co ions drives the reconstruction of the Co3d orbital, resulting in bonding d_{xz}/d_{yz} and d_{z^2} orbitals with reduced energy below the in-plane d_{xy} and $d_{x^2-y^2}$ orbitals (see Figure 5c), which is consistent with the XLD results. In addition, antibonding d_{xz}/d_{yz} states emerge near the Fermi level, which significantly narrows the bandgap compared with STO/LCO SLs and reveals half-metal features. Intriguingly, our calculations further indicate orbital order and charge order in the ground state of S_5L_1, which needs to be further experimentally confirmed.

3. Discussion and Conclusion

The introduction of electron-rich 5d SIO is vital for realizing the fully HS state and thus strong ferromagnetism in LCO monolayer. First, at the LCO/SIO interface, charge-transfer-induced Ir^{5+} can pull harder on O^{2-} compared with Co^{3+},[12b,28] causing O^{2-} away from Co^{3+} ions thus anomalously elongates the *c*-axis, as revealed by the HAADF-STEM results (see Figure 4b). Together with in-plane tensile strain, the Δ_{CF} can be reduced significantly thereby annihilating LS Co^{3+} and promoting fully HS state. Second, the reduction in dimensionality enhances the strength of electron correlations, leading to a preferred population at different orbitals in order to minimize the Coulomb repulsion through spatial avoidance thereby favoring HS state.[29] For instance, the non-charge-transferred LCO monolayer T_5L_1 exhibits more (less) HS Co^{3+} (LS Co^{3+}) than the bulk-like LCO counterparts S_5L_{10} (see Table S1, Supporting Information). In addition, SOC may also play a role in stabilizing HS state. LS Co^{3+} ions exhibit weak SOC, which makes them unfavorable for survival in the presence of SIO slabs with strong SOC.

The pronounced enhancement of SOC in LCO monolayer, on the one hand, could be attributed to the proximity effect from SIO with strong SOC[30]; and on the other hand, it can be contributed by Rashba-like effect from the interfacial built-in electric field (*E*: $SIO^+ \rightarrow LCO^-$) due to charge transfer. Notably, the enhancement of SOC plays an essential role in stabilizing the ferromagnetism of LCO monolayer by supplying magnetic anisotropy so as counteracting Mermin–Wagner restriction,[21b] as indicated by

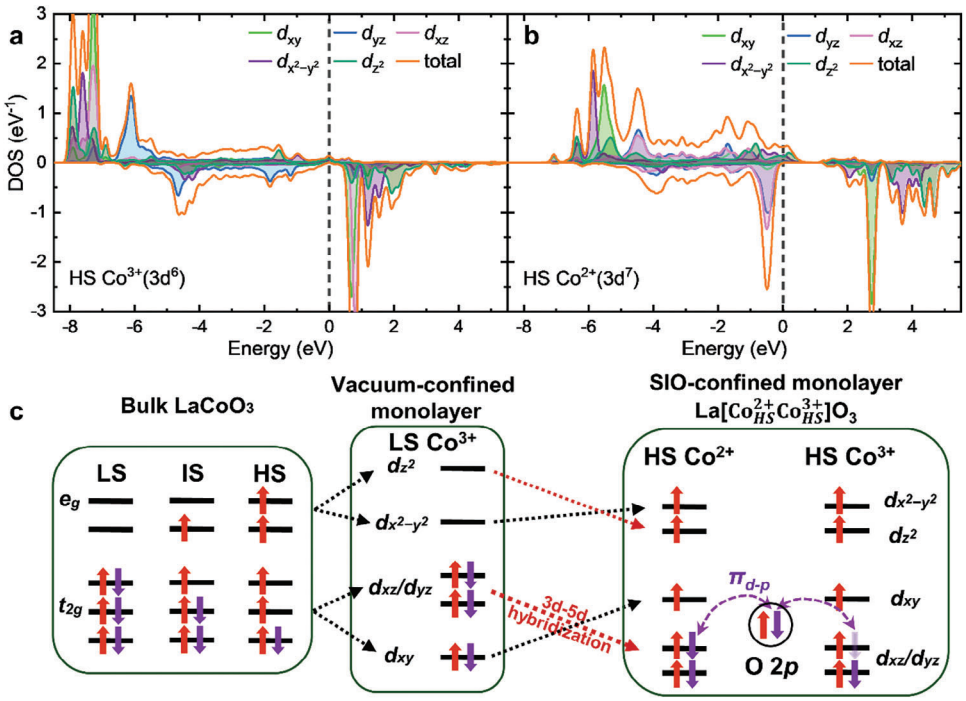

Figure 5. Theoretical calculations using DFT+U. DOS of HS Co^{3+} and HS Co^{2+} are shown in (a) and (b), respectively. c) Schematic of the energy-level distribution of Co3d in LCO under different cases. Left panel are for bulk LCO, where LS, IS, and HS configurations are shown here. Vacuum-confined LCO monolayer (middle panel) possesses a LS configuration due to the confinement effect. Fully HS state with the coexistence of Co^{2+} and Co^{3+} is shown in right panel. Double exchange interaction between HS Co^{2+} and HS Co^{3+} is mediated by t_{2g} (d_{xz}/d_{yz}) electron via Co—O $\pi_{d\text{-}p}$ bond, which causes ferromagnetism in LCO monolayer.

some 2D van der Waals ferromagnets.[21a,31] The ferromagnetic order in such an aliovalent HS Co^{2+}/HS Co^{3+} system is governed by the double-exchange interaction. Different from the manganates where ferromagnetism is mediated by e_g orbital through "head-to-head" σ overlap,[32] the exchange in $La[Co^{3+}_{HS}, Co^{2+}_{HS}]O_3$ is mediated by t_{2g} orbital through Co3d-O2p "shoulder-to-shoulder" π ($\pi_{d\text{-}p}$) overlap (see the right panel in Figure 5c), similar to the case in hole-doped counterpart $La_{0.7}Sr_{0.3}CoO_3$ film.[11a]

In summary, we demonstrated that, by constructing 3d/5d heterointerfaces, an unprecedented fully HS state was realized in SIO-confined LCO monolayer. Such an emergent spin state synergistically exists with ferromagnetic order and large orbital polarization, sharply contrasting with the trivial STO-confined LCO monolayer. Attributed to the strong SOC and the enhanced exchange interactions caused by valence mixture, the ferromagnetic order survives above 100 K, showing the highest Curie temperature and largest atomic moment (≈1.8μ_B/Co) compared to any previous oxide-based 2D ferromagnets. The orbital reconstruction, driven by interfacial 3d-5d hybridization, exhibits a reversal of the Co3d levels that goes beyond the expectations derived from crystal field physics. The strong SOC, which collaborates with the broken inversion symmetry at interface, likely provides significant antisymmetric exchange coupling effect such as Dzyaloshinskii–Moriya interaction,[33] thereby possibly exhibiting a promising host for searching for 2D skyrmion-like spin texture.[34] Besides, such a stacking of heavy-metal layer/2D ferromagnet heterostructure (SIO/LCO) can serve as the base material of potential ultra-compact devices for spintronic applications.[35]

4. Experimental Section

Sample Growth: The SIO/LCO and LCO/STO superlattices were grown on TiO_2-terminated $SrTiO_3$ (001) substrates by Laser molecular beam epitaxy (Laser-MBE, $\lambda = 248$ nm) assisted by in situ reflection high energy electron diffraction (RHEED). The TiO_2-terminated $SrTiO_3$ (001) substrate were obtained by etching with standard buffered oxide etch (BOE) solution and subsequent annealing at 950 °C for 90 min. Laser fluence and repetition rate during growth were 1.1 J cm^{-2} and 4 Hz, respectively. Typical substrate temperature was 660 °C and the oxygen partial pressure was 0.15 mbar. The thickness of each sub-layer was precisely monitored by in situ RHEED. A series of superlattices S_mL_n with m = 1, 5 uc and n = 1–10 uc were prepared using two-target growth alternating $LaCoO_3$ and $SrIrO_3$. S_1L_1 possesses 20 periodic repetitions in order to facilitate XRD measurements, while the other samples all keep ten repetitions. Superlattices for structure characterization and magnetization measurement were capped by ≈4 nm amorphous STO (*a*-STO) in order to protect the periodic superlattices structure. The SIO/LCO (STO/LCO) superlattices for synchrotron X-ray experiment were terminated by additional crystalline SIO (STO) layer for preventing phase decomposition of LCO to be probed.

Structural Characterization: Surface morphology was recorded by atomic force microscope (AFM). X-ray diffraction (XRD), reflectivity (XRR) and reciprocal space mapping (RSM) measurements were carried out for characterizing the crystal structure, crystallinity and orientation by using a high resolution X-ray diffractometer (Malvern PANalytical). The XRR data were fitted using the chemical depth profiles by GenX software. The microscopic chemical configuration of superlattices was measured by High-angle annular dark-field scanning transmission electron microscopy (HAADF-STEM). The cross-section specimens of S_5L_1 and S_1L_1 were prepared by mechanical grinding then Ar ion beam milling. The atom positions were determined by fitting with 2D Gaussian peaks using a MATLAB code.[36] Then the lattice parameter along *c*-axis (d_c) can be estimated as

the distance between two neighboring A-site atoms (including La–La, La–Sr, and Sr–Sr pairs).

Magnetization and Transport Characterization: Both in-plane and out-of-plane field-dependent magnetization were measured by MPMS 3 (Quantum Design), where the sample was loaded by a standard quartz paddle holder. The actual sample magnetization was acquired by subtracting a linear diamagnetic contribution from the STO substrate. Electrical transport measurements were based on the van der Pauw method using a PPMS-9T (Quantum Design). The Hall signals are "odd" with respect to the applied field, thus they were calculated as $R_{xy} = (R_{xy}^{raw}(H) - R_{xy}^{raw}(-H))/2$. Then, the anomalous Hall effect (R_{AHE}) could be obtained by deducting the ordinary Hall effect (R_{OHE}), i.e., $R_{AHE} = R_{xy} - R_{OHE}$. Due to the field is insufficient to saturate the Hall hysteresis, conventionally sweeping field at a fixed temperature can only produce an undesired minor Hall hysteresis without saturating the sample and quenching the magnetic domains. In order to trace the correct major Hall hysteresis, one has to quench the domains by thermal heating and cooling, where the detailed measurement see ref. [37]

Synchrotron X-Ray Experiment: X-ray absorption spectroscopy (XAS) and magnetic circular dichroism (XMCD) were conducted at the Boreas beamline of ALBA Synchrotron Light Source.[38] The measurements were performed under 6 T at 10 K, with the incoming X-ray and magnetic field perpendicular to the sample plane. Resonant soft X-ray reflectometry (RSXR) spectra were measured at the REIXS beamline of the Canadian Light Source (CLS) with a magnetic field (0.6 T) parallel to the sample plane. The samples were aligned with their surface normal in the scattering plane and measured at 20 and 100 K. The measurements were carried out in the specular reflection geometry with several non-resonant photon energies as well as energies at the Co-$L_{2,3}$ resonance (≈765–805 eV). The X-ray linear dichroism (XLD) of S_5L_1 was measured at the CLS as well as Hefei Light Source, and XLD of T_5L_1 was measured at Hefei Light Source. For XLD measurement, the incident X-ray was at 90° and 25° angles to the sample plane at Hefei Light Source, and the X-ray was at the grazing angle of 25° at the CLS where measuring by varying the linear polarization. All X-ray absorption experiments data was recorded using a mode of total electron yield. X-ray photoelectron spectroscopy (XPS) was measured by an in-house photoelectron spectrometer (Thermo Scientific ESCALAB 250Xi) with ultimate vacuum pressure of 5×10^{-10} mbar. The Al Kα X-ray monochromator was operated with an anode power of 150 W.

DFT Calculations: The DFT+U method[39] was employed to investigate the electronic and magnetic properties of $(SrIrO_3)_5/(LaCoO_3)_1$ and $(SrTiO_3)_5/(LaCoO_3)_1$ superlattices using GGA-PBE correlation-exchange functional.[40] All first-principles calculations were performed within the Vienna Ab Initio Simulation Package (VASP) and Wien2k codes. More details see Note S10 (Supporting Information).

Supporting Information

Supporting Information is available from the Wiley Online Library or from the author.

Acknowledgements

The authors thank Dr. Xuguang Liu from Instruments Center for Physical Science, USTC for assistance in macroscopic magnetic measurements. This work was supported by the National Key R&D Program of China (No. 2022YFA1403000) and the National Natural Science Foundation of China (Nos. 52272095 and 11974325). K.C. acknowledges support from the Collaborative Innovation Program of Hefei Science Center, CAS (No. CX2310000177), the National Natural Science Foundation of China (No. 12275272) and the Fundamental Research Funds for the Central Universities (Nos. wk2310000104 and wk2310000106). Q.Z. acknowledges support from the National Natural Science Foundation of China (Nos. 52072400, 52025025 and 51991344), the Beijing Natural Science Foundation (No. Z190010) and the National Key R&D Program of China (No. 2019YFA0308500). Part of the research described in this paper was performed at the Canadian Light Source, a national research facility of the University of Saskatchewan, which is supported by the Canada Foundation for Innovation (CFI), the Natural Sciences and Engineering Research Council (NSERC), the National Research Council Canada (NRC), the Canadian Institutes of Health Research (CIHR), the Government of Saskatchewan, and the University of Saskatchewan. The authors would like to thank the BOREAS beamline of the ALBA Synchrotron Light Facility with the collaboration of ALBA staff (beamtime proposal 2022025648) and MCD-A and MCD-B (Soochow Beamline for Energy Materials) beamlines of NSRL for the synchrotron beamtime.

Conflict of Interest

The authors declare no conflict of interest.

Author Contributions

J.L., L.S., and Q.Z. contributed equally to this work. Z.L., K.C., and R.J.G. conceived the project. J.H. performed the sample preparation, structure and morphology characterization, and magnetic measurements. Q.Z., T.L., M.W., X.Z., P.G., and L.G. performed the HAADF-STEM measurements and atomic position fitting. J.L., K.C., R.J.G., L.H.T., Z.H., X.W., J.F., G.H., R.S., J.H.-M., C.G., and M.V. conducted the synchrotron X-ray experiments and analyzed the results. L.S. performed the DFT+U calculations. G.C. directed the AFM measurement. J.L., L.S., J.Z., Z.L., K.C., and R.J.G. wrote the paper. All authors contributed to the data discussions and analysis.

Data Availability Statement

The data that support the findings of this study are available from the corresponding author upon reasonable request.

Keywords

fully high-spin state, $LaCoO_3$ monolayer, orbital reconstruction, spin-state crossover, strong 2D ferromagnetism

Received: January 30, 2024
Revised: April 22, 2024
Published online:

[1] a) M. W. Haverkort, Z. Hu, J. C. Cezar, T. Burnus, H. Hartmann, M. Reuther, C. Zobel, T. Lorenz, A. Tanaka, N. B. Brookes, H. H. Hsieh, H. J. Lin, C. T. Chen, L. H. Tjeng, *Phys. Rev. Lett.* **2006**, *97*, 176405; b) D. Takegami, A. Tanaka, S. Agrestini, Z. Hu, J. Weinen, M. Rotter, C. Schüßler-Langeheine, T. Willers, T. C. Koethe, T. Lorenz, Y. F. Liao, K. D. Tsuei, H. J. Lin, C. T. Chen, L. H. Tjeng, *Phys. Rev. X* **2023**, *13*, 011037.

[2] a) D. Fuchs, C. Pinta, T. Schwarz, P. Schweiss, P. Nagel, S. Schuppler, R. Schneider, M. Merz, G. Roth, H. v. Löhneysen, *Phys. Rev. B* **2007**, *75*, 144402; b) E.-J. Guo, R. Desautels, D. Lee, M. A. Roldan, Z. Liao, T. Charlton, H. Ambaye, J. Molaison, R. Boehler, D. Keavney, A. Herklotz, T. Z. Ward, H. N. Lee, M. R. Fitzsimmons, *Phys. Rev. Lett.* **2019**, *122*, 187202.

[3] a) S.-Q. Su, S.-Q. Wu, Y.-B. Huang, W.-H. Xu, K.-G. Gao, A. Okazawa, H. Okajima, A. Sakamoto, S. Kanegawa, O. Sato, *Angew. Chem., Int. Ed.* **2022**, *61*, 202208771; b) M. Nadeem, J. Cruddas, G. Ruzzi, B. J. Powell, *J. Am. Chem. Soc.* **2022**, *144*, 9138.

[4] a) J. W. Freeland, J. X. Ma, J. Shi, *Appl. Phys. Lett.* **2008**, *93*, 212501; b) S. Chikara, J. Gu, X. G. Zhang, H.-P. Cheng, N. Smythe, J. Singleton, B. Scott, E. Krenkel, J. Eckert, V. S. Zapf, *Nat. Commun.* **2019**, *10*, 4043.
[5] E. Ruiz, *Phys. Chem. Chem. Phys.* **2014**, *16*, 14.
[6] A. Köbke, F. Gutzeit, F. Röhricht, A. Schlimm, J. Grunwald, F. Tuczek, M. Studniarek, D. Longo, F. Choueikani, E. Otero, P. Ohresser, S. Rohlf, S. Johannsen, F. Diekmann, K. Rossnagel, A. Weismann, T. Jasper-Toennies, C. Näther, R. Herges, R. Berndt, M. Gruber, *Nat. Nanotechnol.* **2020**, *15*, 18.
[7] J.-F. Lin, V. V. Struzhkin, S. D. Jacobsen, M. Y. Hu, P. Chow, J. Kung, H. Liu, H.-k. Mao, R. J. Hemley, *Nature* **2005**, *436*, 377.
[8] a) K. S. Kumar, M. Ruben, *Angew. Chem., Int. Ed.* **2021**, *60*, 7502; b) O. Kahn, C. J. Martinez, *Science* **1998**, *279*, 44; c) S. P. Vallone, A. N. Tantillo, A. M. dos Santos, J. J. Molaison, R. Kulmaczewski, A. Chapoy, P. Ahmadi, M. A. Halcrow, K. G. Sandeman, *Adv. Mater.* **2019**, *31*, 1807334.
[9] a) W. S. Choi, J.-H. Kwon, H. Jeen, J. E. Hamann-Borrero, A. Radi, S. Macke, R. Sutarto, F. He, G. A. Sawatzky, V. Hinkov, M. Kim, H. N. Lee, *Nano Lett.* **2012**, *12*, 4966; b) V. Chaturvedi, S. Ghosh, D. Gautreau, W. M. Postiglione, J. E. Dewey, P. Quarterman, P. P. Balakrishnan, B. J. Kirby, H. Zhou, H. Cheng, A. Huon, T. Charlton, M. R. Fitzsimmons, C. Korostynski, A. Jacobson, L. Figari, J. G. Barriocanal, T. Birol, K. A. Mkhoyan, C. Leighton, *Nat. Commun.* **2022**, *13*, 7774; c) P. M. Raccah, J. B. Goodenough, *Phys. Rev.* **1967**, *155*, 932; d) M. A. Korotin, S. Y. Ezhov, I. V. Solovyev, V. I. Anisimov, D. I. Khomskii, G. A. Sawatzky, *Phys. Rev. B* **1996**, *54*, 5309; e) Y. Yokoyama, Y. Yamasaki, M. Taguchi, Y. Hirata, K. Takubo, J. Miyawaki, Y. Harada, D. Asakura, J. Fujioka, M. Nakamura, H. Daimon, M. Kawasaki, Y. Tokura, H. Wadati, *Phys. Rev. Lett.* **2018**, *120*, 206402.
[10] Z. Hu, H. Wu, M. W. Haverkort, H. H. Hsieh, H. J. Lin, T. Lorenz, J. Baier, A. Reichl, I. Bonn, C. Felser, A. Tanaka, C. T. Chen, L. H. Tjeng, *Phys. Rev. Lett.* **2004**, *92*, 207402.
[11] a) D. Fuchs, M. Merz, P. Nagel, R. Schneider, S. Schuppler, H. von Löhneysen, *Phys. Rev. Lett.* **2013**, *111*, 257203; b) J. S. Zhou, J. Q. Yan, J. B. Goodenough, *Phys. Rev. B* **2005**, *71*, 220103.
[12] a) X.-j. Li, B.-T. Wang, W. Yin, *J. Magn. Magn. Mater.* **2022**, *555*, 169318; b) C. F. Chang, Z. Hu, H. Wu, T. Burnus, N. Hollmann, M. Benomar, T. Lorenz, A. Tanaka, H. J. Lin, H. H. Hsieh, C. T. Chen, L. H. Tjeng, *Phys. Rev. Lett.* **2009**, *102*, 116401; c) S. Li, J. Wang, Q. Zhang, M. A. Roldan, L. Shan, Q. Jin, S. Chen, Z. Wu, C. Wang, C. Ge, M. He, H. Guo, L. Gu, K.-j. Jin, E.-J. Guo, *Phys. Rev. Mater.* **2019**, *3*, 114409.
[13] D. Meng, H. Guo, Z. Cui, C. Ma, J. Zhao, J. Lu, H. Xu, Z. Wang, X. Hu, Z. Fu, R. Peng, J. Guo, X. Zhai, G. J. Brown, R. Knize, Y. Lu, *Proc. Natl. Acad. Sci., USA* **2018**, *115*, 2873.
[14] N. Hollmann, Z. Hu, M. Valldor, A. Maignan, A. Tanaka, H. H. Hsieh, H. J. Lin, C. T. Chen, L. H. Tjeng, *Phys. Rev. B* **2009**, *80*, 085111.
[15] R. Ramesh, D. G. Schlom, *Nat. Rev. Mater.* **2019**, *4*, 257.
[16] H. Y. Hwang, Y. Iwasa, M. Kawasaki, B. Keimer, N. Nagaosa, Y. Tokura, *Nat. Mater.* **2012**, *11*, 103.
[17] a) J. Liu, X. Zhang, Y. Ji, X. Gao, J. Wu, M. Zhang, L. Li, X. Liu, W. Yan, T. Yao, Y. Yin, L. Wang, H. Guo, G. Cheng, Z. Wang, P. Gao, Y. Wang, K. Chen, Z. Liao, *J. Phys. Chem. Lett.* **2022**, *13*, 11946; b) X. Liu, M. Kotiuga, H. S. Kim, A. T. N'Diaye, Y. Choi, Q. Zhang, Y. Cao, M. Kareev, F. Wen, B. Pal, J. W. Freeland, L. Gu, D. Haskel, P. Shafer, E. Arenholz, K. Haule, D. Vanderbilt, K. M. Rabe, J. Chakhalian, *Proc. Natl. Acad. Sci., USA* **2019**, *116*, 19863; c) S. Agrestini, K. Chen, C. Y. Kuo, L. Zhao, H. J. Lin, C. T. Chen, A. Rogalev, P. Ohresser, T. S. Chan, S. C. Weng, G. Auffermann, A. Völzke, A. C. Komarek, K. Yamaura, M. W. Haverkort, Z. Hu, L. H. Tjeng, *Phys. Rev. B* **2019**, *100*, 014443.
[18] Z. Zhong, P. Hansmann, *Phys. Rev. X* **2017**, *7*, 011023.
[19] S. C. Haw, Z. Hu, H. J. Lin, J. M. Lee, H. Ishii, N. Hiraoka, A. Meléndez-Sans, A. C. Komarek, L. H. Tjeng, K. Chen, C. Luo, F. Radu, C. T. Chen, J.-M. Chen, *J. Alloys Compd.* **2021**, *862*, 158050.
[20] a) M. Huijben, L. W. Martin, Y. H. Chu, M. B. Holcomb, P. Yu, G. Rijnders, D. H. A. Blank, R. Ramesh, *Phys. Rev. B* **2008**, *78*, 094413; b) J. Xia, W. Siemons, G. Koster, M. R. Beasley, A. Kapitulnik, *Phys. Rev. B* **2009**, *79*, 140407(R).
[21] a) C. Gong, X. Zhang, *Science* **2019**, *363*, eaav4450; b) N. D. Mermin, H. Wagner, *Phys. Rev. Lett.* **1966**, *17*, 1133.
[22] S. Rom, S. Baidya, S. Bhattacharjee, T. Saha-Dasgupta, *Appl. Phys. Lett.* **2023**, *122*, 021602.
[23] D. Shin, S. Yoon, S. Song, S. Park, H. N. Lee, W. S. Choi, *Adv. Mater. Interfaces* **2022**, *9*, 2200433.
[24] Z. Liao, M. Huijben, Z. Zhong, N. Gauquelin, S. Macke, R. J. Green, S. Van Aert, J. Verbeeck, G. Van Tendeloo, K. Held, G. A. Sawatzky, G. Koster, G. Rijnders, *Nat. Mater.* **2016**, *15*, 425.
[25] S. Lee, A. T. Lee, A. B. Georgescu, G. Fabbris, M.-G. Han, Y. Zhu, J. W. Freeland, A. S. Disa, Y. Jia, M. P. M. Dean, F. J. Walker, S. Ismail-Beigi, C. H. Ahn, *Phys. Rev. Lett.* **2019**, *123*, 117201.
[26] G. van der Laan, B. T. Thole, *Phys. Rev. Lett.* **1988**, *60*, 1977.
[27] a) P. Carra, B. T. Thole, M. Altarelli, X. Wang, *Phys. Rev. Lett.* **1993**, *70*, 694; b) B. T. Thole, P. Carra, F. Sette, G. van der Laan, *Phys. Rev. Lett.* **1992**, *68*, 1943.
[28] S. Agrestini, C. Y. Kuo, D. Mikhailova, K. Chen, P. Ohresser, T. W. Pi, H. Guo, A. C. Komarek, A. Tanaka, Z. Hu, L. H. Tjeng, *Phys. Rev. B* **2017**, *95*, 245131.
[29] L. Qiao, J. H. Jang, D. J. Singh, Z. Gai, H. Xiao, A. Mehta, R. K. Vasudevan, A. Tselev, Z. Feng, H. Zhou, S. Li, W. Prellier, X. Zu, Z. Liu, A. Borisevich, A. P. Baddorf, M. D. Biegalski, *Nano Lett.* **2015**, *15*, 4677.
[30] a) J. Matsuno, N. Ogawa, K. Yasuda, F. Kagawa, W. Koshibae, N. Nagaosa, Y. Tokura, M. Kawasaki, *Sci. Adv.* **2016**, *2*, 1600304; b) A. Avsar, J. Y. Tan, T. Taychatanapat, J. Balakrishnan, G. K. W. Koon, Y. Yeo, J. Lahiri, A. Carvalho, A. S. Rodin, E. C. T. O'Farrell, G. Eda, A. H. Castro Neto, B. Özyilmaz, *Nat. Commun.* **2014**, *5*, 4875.
[31] a) A. Bedoya-Pinto, J.-R. Ji, A. K. Pandeya, P. Gargiani, M. Valvidares, P. Sessi, J. M. Taylor, F. Radu, K. Chang, S. S. P. Parkin, *Science* **2021**, *374*, 616; b) C. Gong, L. Li, Z. Li, H. Ji, A. Stern, Y. Xia, T. Cao, W. Bao, C. Wang, Y. Wang, Z. Q. Qiu, R. J. Cava, S. G. Louie, J. Xia, X. Zhang, *Nature* **2017**, *546*, 265; c) B. Huang, G. Clark, E. Navarro-Moratalla, D. R. Klein, R. Cheng, K. L. Seyler, D. Zhong, E. Schmidgall, M. A. McGuire, D. H. Cobden, W. Yao, D. Xiao, P. Jarillo-Herrero, X. Xu, *Nature* **2017**, *546*, 270; d) J. L. Lado, J. Fernández-Rossier, *2D Mater.* **2017**, *4*, 035002.
[32] T. Kimura, Y. Tokura, *Annu. Rev. Mater. Sci.* **2000**, *30*, 451.
[33] S. G. Jeong, J. Y. Oh, L. Hao, J. Liu, W. S. Choi, *Adv. Funct. Mater.* **2023**, *33*, 2301770.
[34] A. Fert, N. Reyren, V. Cros, *Nat. Rev. Mater.* **2017**, *2*, 17031.
[35] a) L. Liu, Q. Qin, W. Lin, C. Li, Q. Xie, S. He, X. Shu, C. Zhou, Z. Lim, J. Yu, W. Lu, M. Li, X. Yan, S. J. Pennycook, J. Chen, *Nat. Nanotechnol.* **2019**, *14*, 939; b) T. Nan, T. J. Anderson, J. Gibbons, K. Hwang, N. Campbell, H. Zhou, Y. Q. Dong, G. Y. Kim, D. F. Shao, T. R. Paudel, N. Reynolds, X. J. Wang, N. X. Sun, E. Y. Tsymbal, S. Y. Choi, M. S. Rzchowski, Y. B. Kim, D. C. Ralph, C. B. Eom, *Proc. Natl. Acad. Sci., USA* **2019**, *116*, 16186.
[36] Y. Sun, A. Y. Abid, C. Tan, C. Ren, M. Li, N. Li, P. Chen, Y. Li, J. Zhang, X. Zhong, J. Wang, M. Liao, K. Liu, X. Bai, Y. Zhou, D. Yu, P. Gao, *Sci. Adv.* **2019**, *5*, eaav4355.
[37] a) X. Liu, S. Fang, Y. Fu, W. Ge, M. Kareev, J.-W. Kim, Y. Choi, E. Karapetrova, Q. Zhang, L. Gu, E.-S. Choi, F. Wen, J. H. Wilson, G. Fabbris, P. J. Ryan, J. W. Freeland, D. Haskel, W. Wu, J. H. Pixley, J. Chakhalian, *Phys. Rev. Lett.* **2021**, *127*, 277204; b) J. Liu, X. Gao, K. Shi, M. Zhang, J. Wu, V. Ukleev, F. Radu, Y. Ji, Z. Deng, L. Wei, Y. Hong, S. Hu, W. Xiao, L. Li, Q. Zhang, Z. Wang, L. Wang, Y. Gan, K. Chen, Z. Liao, *Nano Lett.* **2024**, *24*, 1351.

[38] A. Barla, J. Nicolás, D. Cocco, S. M. Valvidares, J. Herrero-Martín, P. Gargiani, J. Moldes, C. Ruget, E. Pellegrin, S. Ferrer, *J. Synchrotron Radiat.* **2016**, *23*, 1507.
[39] a) P. Hohenberg, W. Kohn, *Phys. Rev.* **1964**, *136*, B864; b) V. I. Anisimov, J. Zaanen, O. K. Andersen, *Phys. Rev. B* **1991**, *44*, 943.
[40] J. P. Perdew, K. Burke, M. Ernzerhof, *Phys. Rev. Lett.* **1996**, *77*, 3865.